Comparative studies of CO$_2$ capture using acid and base modified activated carbon from sugarcane bagasse

Mohammed Alhassan, Iwodi Andrew, Manase Auta, Musa Umaru, Mohammed Umar Garba, Abubakar G. Isah & Bello Alhassan

Published online: 10 Apr 2017.

Submit your article to this journal ⏎

View related articles ⏎

View Crossmark data ⏎

Taylor & Francis
Taylor & Francis Group

Check for updates

Comparative studies of CO_2 capture using acid and base modified activated carbon from sugarcane bagasse

Mohammed Alhassan[a], Iwodi Andrew[a], Manase Auta[a], Musa Umaru[a], Mohammed Umar Garba[a], Abubakar G. Isah[a] and Bello Alhassan[b]

[a]Chemical Engineering Department, Federal University of Technology, Minna, Nigeria; [b]Entrepreneurship Development Centre, Kwara State Polytechnic, Ilorin, Nigeria

ABSTRACT

This study reports the potential of acid and base modified sugarcane bagasse activated carbon for carbon dioxide (CO_2) adsorption. The rate of CO_2 adsorption by the unmodified (UMAC), acid (AMAC) and base modified activated carbon (BMAC) was determined gravimetrically via weight differential measurement. Surface morphology and functional group of the adsorbent before and after adsorption were also determined. The adsorbents performance was evaluated using a cylindrical glass column equipped with a digital weighing balance. Characterization of adsorbents showed that BMAC had a better pore structure thereby making it the most effective adsorbent for CO_2. CO_2 adsorption increased over time in the order UMAC < AMAC < BMAC. The highest amount (148.5 mg.g^{-1}) of CO_2 was adsorbed at 25°C and 25 min. The adsorption kinetics followed second-order kinetics with a regression coefficient (R^2) of 0.9967. The activation energy (E_a) of the process was evaluated to be 5.77, 13.02 and 13.55 kJ.mol^{-1} for BMAC, AMAC and UMAC respectively. The low E_a observed suggests that CO_2 is weakly bonded to the adsorbent surface. The acid and base modified sugarcane bagasse activated carbon produced is characterized with enhanced capacity for CO_2 adsorption.

Introduction

Carbon (IV) oxide (CO_2) is a greenhouse gas. Studies have shown that the release of CO_2 from the combustion of fossil fuels is a principal contributor to global warming and climate change [1]. With the present increase in human population and concurrent energy demands, the rate of CO_2 release into the atmosphere is expected to increase proportionally with the burning of fossil fuels. It has been reported that power generation plants account for one-third of the CO_2 released globally [2,3]. The concentration of CO_2 in the atmosphere was projected to increase from pre-industrial concentration of 270 ppm to 700 ppm by the year 2010 [4]. D'Alessandro et al., [5] stated that if major preventive measures are not put in place to curtail this increase, this situation will essentially lead to a significant increase in global mean temperatures thereby endangering the biotic environment. To reduce CO_2 emissions to 6% below 1990's level, commitments were made by several countries during the United Nations Framework Convention on Climate Change (UNFCC) held in Kyoto [4]. CO_2 emissions from power plants can be effectively reduced through many techniques which include in situ concentration, fuel conversion process, and extraction and sequestration from flue gases generated during fuel conversion processes.

Chemical solvents and physical adsorption method are most commonly used in the latter methods [3].

Amine based adsorbents are commonly used for CO_2 capture. These adsorbents are associated with a number of problems such as high regeneration energy demand, corrosive tendency and degradation of amines [6]. The selection of separation process which is determined by adsorption and diffusion activity inherent in most activated carbon materials also limits their applications [5,7,8]. Therefore, there is a need to develop materials whose diffusivity and adsorption selectivity can be independently tuned at a molecular level. The relative abundance, low cost, minimal sensitivity to moisture and high thermal stability are distinctive characteristics of activated carbons which have continuously placed it in a vantage position as an exceptionally viable adsorbent for CO_2 sequestration [7,9].

Many studies have documented the use of activated carbon for CO_2 capture. Alhasan et al. [9] reported the use of amine-impregnated *Jatropha curcas* shell activated carbon for CO_2 capture and observed high adsorption capacity from the modified adsorbent. Ketcha et al. [10] developed a maize cob activated carbon for CO_2 adsorption; the author reported that the hard part of the cob gave a better activated carbon with good adsorption properties. Tsai et al. [11,12],

---

CONTACT Mohammed Alhassan ✉ moh.alhass@futminna.edu.ng; mohakusi2003@yahoo.com

Chang et al. [13] and Boudrahem et al. [14] produced activated carbon from maize cobs but their methodological approaches differ from that of Ketcha et al. [10]. Rashidi et al. [8] developed activated carbon from coconut shells and found the adsorption capacity of the optimized coconut shell to be almost the same as commercially activated carbon at 25°C. According to Bansal et al. [15], pore volume, surface area and mean pore diameter of activated carbon are important parameters and depend on carbonization and activation conditions such as heating rate, temperature, holding time and type of activating agent.

Phosphoric acid and sodium hydroxide as acidic and basic activating agents have been known to produce activated carbon with a highly developed porous structure and reduced tar formation when used for activation of lignocellulose material due to their dehydrogenation properties [16,17]. There is no documented evidence on the use of acid and base functionalized sugarcane bagasse activated carbon for CO_2 capture and sequestration. This work is therefore aimed at developing acid (phosphoric) and base (sodium hydroxide) functionalized sugarcane bagasse activated carbon for CO_2 capture and sequestration.

Methodology

Materials

Sugarcane bagasse was obtained from a sugarcane depot at Kpakungu, a satellite town in Minna, Niger State, where heaps of the waste sugarcane bagasse from a variety of sugarcane grown in Nigeria (S9Co959 and S27BC0997) can be found. Analytical grade zinc chlorine ($ZnCl_2$), phosphoric acid (H_3PO_4) and sodium hydroxide (NaOH) were obtained from Sigma Aldrich, UK.

Synthesis of activated carbons from sugarcane bagasse

The bagasse was washed thoroughly to remove impurities. The bagasse was dried in an oven at 110°C until constant weight was attained. A sieve stack was arranged so as to obtain a particle size fraction of 0.18–1.18 mm. ASTM E828 procedure was followed to determine the particle size distribution [18]. Table 1 shows particle size distribution of the sugarcane bagasse

used in this research. It can be observed from Table 1 that the bulk of sugarcane particles (87.87%) were retained within these screen size range, while 10.88% was obtained below 0.18 mm screen size. Particle size fraction of 0.18–1.18 mm of raw sugarcane bagasse was used in the production of the activated carbon.

A known quantity (2000 g) of the dried sample was placed inside a crucible and placed in the furnace. The furnace was tightly closed to avoid passage of air in the presence of nitrogen. The furnace was set to 680°C for 60 min. The sample was heated at a heating rate of 10°C.min^{-1} and held at 680°C for 1 h, after which the sample was removed using tongs. The carbonized sample was allowed to cool for 15 min in a closed container to avoid exposure to air. Then 320.87 g of the carbonized sample was measured and activated with one molar (1M) solution of zinc chloride ($ZnCl_2$) solution. The solution was properly mixed to form a paste at the reagent to sample ratio of 1:1. After activation, the samples were left for 48 h for effective penetration of reagent into the pores of the samples. The samples were washed thoroughly to remove excess salt until the pH was stable. The washed samples were oven dried for 5 h at 110°C to give unmodified activated carbon (UMAC). Then 50 g of the UMAC was measured with one molar (1M) solution of phosphoric acid (H_3PO_4). It was properly mixed with a reagent to sample ratio of 1:1 to form a paste. The sample was left for 48 h for effective penetration of reagent into the pores of the carbon. It was washed thoroughly to remove excess salt until the pH stabilized. The washed sample was oven dried for 5 h at 110°C to give acid modified activated carbon (AMAC) for adsorption studies and characterization. Further, 50 g of UMAC was measured with one molar (1M) solution of sodium hydroxide (NaOH) and was properly mixed at a reagent to sample ratio of 1:1 to form a paste. The sample was left for 48 h for effective penetration of reagent into the pores of the UMAC. The sample was washed thoroughly to remove excess salt until the pH was stable. The washed sample was oven dried for 5 h at 110°C to give base modified activated carbon (BMAC) for adsorption studies and characterization.

Characterization of raw sugarcane bagasse and activated carbon

Thermal analysis was performed on the raw sugar cane using a thermal analyzer (Mettler Toledo TGA/STDA 851). The moisture, volatile matter and ash content of the raw sugarcane bagasse and the activated carbon produced were determined using ASTM E871, ASTM E872 and ASTM D1102 respectively. Both the elemental and oxide compositions of the samples were determined using XRF-Thermoscientific Advant'x 1200 Model. A Shimadzu 6000 model X-ray diffraction machine was used to record the X-ray diffraction pattern of the samples of the

Table 1. Particle size distribution determined by sieve analysis of oven-dried sugarcane bagasse.

Screen size (mm)	Average mass fraction (%)	SD
2.36	1.25	0.000577
1.18	32.08	0
0.6	21.20	0.001155
0.18	34.59	0.001155
0.15	8.62	0.000577
0.075	2.08	0.000577
0	0.18	0.000577
	100	

activated carbon produced at a scan rate of 2–100° per min. The pronounced peaks or diffractograms displayed express the samples composition at the various angles of the degree 2-theta. The surface morphology of the activated carbon was analyzed using JEOL JSM-7600F. SEM Test Method (ASTM B487) was used. The functional groups in the raw sugar cane bagasse and activated carbons produced were determined using Fourier infrared spectroscopy (FTIR) model FTIR-8400s (Shimadzu). FTIR spectra were obtained from all samples.

Determination of the physical parameters of activated carbon

Yield and burn off
Burn off and yield were calculated using Equations (1) and (2) [19]:

$$\%Burn\ off = \frac{W_b - W_a}{W_b} \times 100 \quad (1)$$

$$\%Yield = \frac{W_a}{W_c} \times 100 \quad (2)$$

where W_a = dry weight before activation, W_b = dry weight after activation and W_c = dry weight of raw material before carbonization.

pH
pH values were determined using ASTM D3838-05 (2011) procedure. Typically, 10 g of the activated carbon prepared was heated in 100 ml distilled water to boiling point for 15 min. The slurry formed was filtered (using filter paper), the filtrate was cooled and its pH was measured using a pH meter.

Pore volume
Four grams of each sample were immersed in 50 ml distilled water in a beaker and boiled for 20 min. This is to displace air in the pores. The samples were filtered and dried, after which they were reweighed and the change in weight divided by 1 g.cm^3 gives the pore volumes.

Surface area
The internal surface area of the activated carbon was determined using Sears method [20,21]. A total of 1.5 g of activated carbon was added to 100 ml of diluted (1M) hydrochloric acid at a pH of 3. Then 30 g of sodium chloride was added and stirred. The suspension was made up to 150 ml with deionized water. The resulting solutions were titrated against NaOH to raise the pH from 4 to 9 and the volume (V) of the titrant was recorded. The surface area according to this method was calculated from Equation (3):

$$S = (32V - 25)\frac{m^2}{g} \quad (3)$$

where S = surface area of the activated carbon, V = volume of sodium hydroxide required to raise the pH of the sample from 4 to 9.

Carbon (IV) oxide adsorption
The CO_2 adsorption column was held by a retort stand with the end of the column connected to a CO_2 delivery pipe from a gas cylinder. The adsorption column was fitted with wire mesh at the bottom, from where the delivery pipe was fixed. The upper part of the column had an exit for excess gas to escape, while the top of the column was firmly corked with a cap. Exactly 2 g UMAC of particle size 0.8–1 mm was poured into the adsorption column and firmly corked. The apparatus was connected to a CO_2 cylinder. The cylinder tap was opened and the gas was released at the rate of 60 ml min^{-1} and held at atmospheric pressure and temperature of 37°C, over time intervals of 5, 10, 15, 20 and 25 min. The weights of the samples were measured with an electronic weighing balance at the intervals to note the difference in weight of the samples until a constant weight, which indicates its maximum adsorption capacity was obtained. The same procedure was repeated for the other samples, AMAC and BMAC.

$$Amount\ of\ CO_2\ Adsorbed = \frac{Qt(mg) - Qo(mg)}{Qo(g)} \quad (4)$$

where Q_0 is the initial weight before absorption and Q_t is the final weight after absorption.

Adsorption kinetics

Lagergren's pseudo-first-order and pseudo-second-order models
Lagergren's pseudo-first-order and pseudo-second-order models were used to test the kinetic behavior in this work and the conformity of the experimental work and kinetic model can be analyzed by the regression coefficient (R^2) values. The linearized Lagergren pseudo-first-order model can generally be expressed by Equation (5) [8]:

$$\log(qe - qt) = \log(qe) - \frac{k1(t)}{2.303} \quad (5)$$

where q_e and q_t are the amount of CO_2 adsorbed in (mg.g^{-1}) at equilibrium and at time t, respectively, and k_1 is the rate constant of pseudo-first-order model (min^{-1}). In addition, the pseudo-second-order model and initial rate of adsorption, h (mg.g^{-1} min^{-1}) according to Rashidi et al. [8] using Equation (6) is:

$$\frac{t}{qt} = \frac{1}{k_2 qe^2} + \frac{1(t)}{qt} \quad (6)$$

$$h = k_2 q_e^2 \qquad (7)$$

If the pseudo-second-order kinetic model is applicable in the adsorption process, a plot of $1/q_t$ against time (t) will result in a straight line with $1/h$ and $1/q_e$ as the y-intercept and slope respectively [8].

Activation energy

The Arrhenius equation shown in Equation (8) can be used to estimate the activation energy of the adsorption process [8,22]:

$$lnk = -\frac{Ea}{RT} + lnk_o \qquad (8)$$

where k is the pseudo-second-order kinetic model rate constant ($g.mg^{-1}min^{-1}$), E_a is the activation energy of the adsorption process ($Jmol^{-1}$), R is the gas constant (8.314 J mol^{-1} K^{-1}), T is the adsorption temperature in Kelvin, and k_o is the temperature independent factor ($g.mg^{-1}min^{-1}$).

Intra-particle diffusion model

Intra-particle diffusion model can be expressed by Equation (9) [23]:

$$q_t = k_{id}t^{\frac{1}{2}} + c_i \qquad (9)$$

where q_t represents the amount of CO_2 adsorbed at any time t ($mg.g^{-1}$), k_{id} is the intra-particle rate constant ($mg/min \cdot t^{1/2}$), and t is the contact time ($min^{1/2}$). A straight linear plot that passes through the origin is observed when the adsorption process obeys the intra-particle diffusion model [8].

Results and discussion

Raw sugarcane bagasse characterization

Table 2 shows the oxide composition of sugarcane bagasse. The oxides were majorly from heavy metals with calcium oxide having the highest percentage of 70.2% followed by silicone, iron and aluminum oxides with percentage values of 16.2, 4.73 and 2.71% respectively. Sodium, manganese, iron, copper, zinc and phosphorus oxides were found in trace amounts. The

Table 2. Mineral oxide composition of sugarcane bagasse.

Mineral oxides	Percentage (%)
P_2O_5	0.59
TiO_2	0.80
Na_2O	1.29
MgO	1.0
CaO	70.2
MnO	0.6
K_2O	2.3
Fe_2O_3	4.73
Al_2O_3	2.71
SiO_2	16.21

oxide content of the bagasse used in this study is comparable with the reported values by Sultana and Rahman [24]. However, the sum of Al_2O_3, SiO_2, and Fe_2O_3, which is less than 70%, suggests that the bagasse is not a pozzolanic material while the presence of these oxides suggests the stability of the bagasse for activated carbon production.

Thermogravimetric and differential thermogravimetric analysis of sugarcane bagasse

Figure 1 shows the thermogravimetric (TG) and differential thermogravimetric (DTG) profile of sugarcane bagasse. The DTG curve indicates three stages of thermal decomposition behavior. From the DTG curve, the first derivative peak temperature (A) was at 105°C. This temperature corresponds to the peak temperature at which drying takes place. On the corresponding DTG, this temperature corresponds to the temperature at which 3% of weight loss occurred which might be due to the moisture being driven off [18]. The second derivative peak temperature (B) on the DTG curve was observed at 250°C, which corresponds to a point on the TG curve where approximately 22% of weight loss was observed. This weight loss, according to Alhassan and Andresen [18], may be due to the removal of water resulting from depolymerization of sugar cane bagasse. The third derivative peak (C) was observed at 350°C, corresponding to a temperature on the TG curve where a weight loss of 67.42% occurred which can be attributed to the breakdown of hemicellulose, cellulose and lignin. No peak emerges after 550°C on the DTG curve which corresponds to the point on the TG where no significant weight loss was observed.

The summation of weight losses observed at peaks A, B and C on the DTG curve which correspond to about 92.42% weight loss from the TG curve can be attributed to the volatile content of the sugar cane bagasse which indicates that sugar cane bagasse is composed largely of volatile matter, which when driven off leaves behind large pore space with high CO_2 adsorption capacity [8]. It can be observed that the thermogravimetric profiles of both the industrial
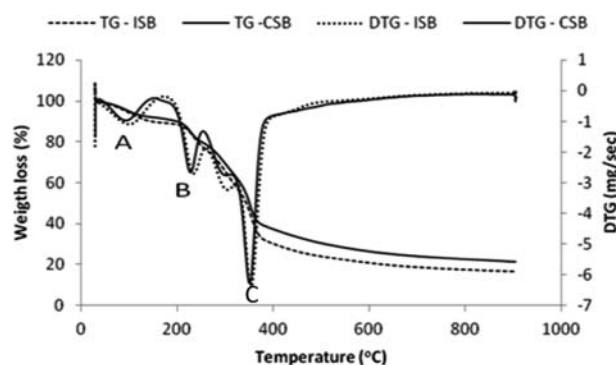

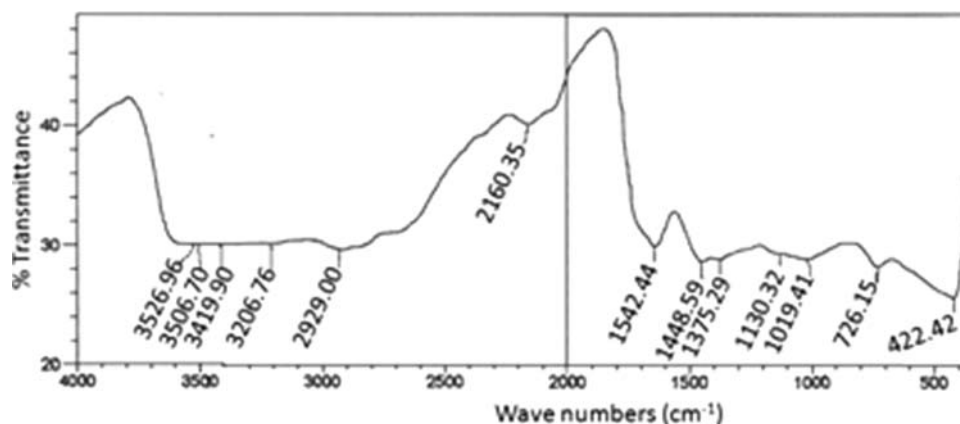**Figure 1.** TG and DTG curves of sugarcane bagasse.

Figure 2. FTIR of sugarcane bagasse.

and the chewing sugar cane bagasse do not differ significantly and hence chewing sugar cane bagasse was selected for use in this research.

Fourier infrared spectroscopy analysis of sugar cane bagasse

Figure 2 shows the FTIR of sugarcane bagasse. Peaks measured were in the range 4000–400 cm^{-1}. Analysis showed the presence of the following functional groups: 726.15 cm^{-1} indicates the presence of alkanes; 1019.41 cm^{-1} and 1130.32 cm^{-1} fall within aliphatic amines; 1375.29 cm^{-1} shows the presence of aromatic amines groups; 2160.35 cm^{-1} shows the presence of alkynes; 3419.90 cm^{-1} shows the presence of primary, secondary and tertiary amines; and 3506.70 cm^{-1} indicates alcohol and phenol functional groups. The acidic functional groups on the carbon surface, such as hydroxyl and carbonyl, were able to attract ammonia molecules [25]. The significance of the presence of amine functional groups is an indication that the sample is a good adsorbent for CO_2 capture since amine functional groups enhance CO_2 adsorption [8].

Physicochemical parameters of activated carbon samples

Table 3 shows the physiochemical characteristics of the adsorbents produced. The surface area was calculated using sears method, and from Table 3 it can be observed that BMAC has a larger surface area of 800.6

Table 3. Physiochemical properties of activated carbon.

Parameters	UMAC	AMAC	BMAC
Yield (%)	19.5	19.5	19.5
Burn off (%)	9.51	9.51	9.51
Surface area (m^2/g)	563.8	602.2	800.6
pH	6.87	3.52	8.87
Moisture content (%)	14.4	9.2	8.4
Ash content (%)	5.0	4.5	3.3
Pore volume (g/cm^3)	0.825	0.842	0.94
Volatile matter (%)	78.9	78.9	78.9
Fixed carbon content (%)	16.1	16.6	17.8

m^2.g^{-1} followed by AMAC with a surface area of 602.2 m^2.g^{-1}. UMAC had the least surface area of 563.8 m^2.g^{-1}. These findings show that BMAC is the best adsorbent out of the three adsorbents prepared. The three adsorbents produced had surface areas higher than the 320 m^2.g^{-1} as reported by Devnarain et al. [26] for activated carbon produced from bagasse under the same carbonization conditions. Smit [27] reported that a high surface area gives high adsorption capacity. Generally, the lower the ash content of a sample the higher its carbon content, which implies high pores and surface area [28]. From this result, UMAC had a higher ash content of 5.0% than AMAC which contains 4.5% of ash while BMAC had the least ash content of 3.3% which means BMAC will be a better adsorbent in terms of the ash content. The ash content obtained in this study for all adsorbents is within the ASTM standard limit of <8%. Since lower ash content implies better activated carbon quality, BMAC is the best adsorbent followed by AMAC and UMAC. From Table 3, it can be observed that the volatile matter for UMAC, AMAC and BMAC was the same (78.9%) which is as expected since they were all produced from the same material at the same experimental conditions. According to Rashidi et al. [29], high volatile matter contributes to increased pore volume. The fixed carbon contents of all samples is usually a function of the volatile matter and the ash content: the lower the ash content the higher the fixed carbon content which leads to an increase in pore and surface area [26]. UMAC had a carbon content of 16.1%, AMAC had 16.6% while BMAC had 17.8%, which shows that BMAC will have a higher pore and surface area which will consequently make a better adsorbent compared to other adsorbents. According to Qureshi [30], the pH of the activated carbon depends on the method employed during preparation and the authors further added that, in some cases, adsorption increases with increase in pH while, in other cases, adsorption decreases with increase in pH value. This phenomenon depends on the nature of the adsorbate, whether it is basic, neutral

or acidic. UMAC showed a pH of 6.87 which is almost neutral, while AMAC showed a value of 3.52 which is acidic, and a value of 8.87 was obtained for BMAC which is basic. Micro-pores constitute the largest proportion of the internal surface of the activated carbon and contribute most to the total pore volume; most gaseous adsorption takes place within these micro-pores [31]. BMAC showed a better porosity of 0.9 cm^3 followed by AMAC with a porosity of 0.842 cm^3 while UMAC had a porosity of 0.825 cm^3. This result indicates that BMAC will be a better adsorbent among the three samples produced because of its high porosity. The percentage yield of the activated carbons produced from sugarcane bagasse were found to be same for all three samples (AMAC, BMAC and UMAC) while the burn-off was found to be 9.15%. The moisture content was 8.4% for BMAC, 9.2% for AMAC and 14.4% for UMAC. The variation in the moisture content could be a result of the interactions of the different reagents used during the modification of the activated carbon samples when the samples were exposed to the atmosphere. The results indicate that BMAC is more hydrophobic than AMAC and UMAC, which reflects its better adsorption capacity.

Carbon dioxide adsorption capacity

From Figure 3, it can be observed that as time increases the adsorption of CO_2 increases up to a time of 20 min. A sharp increase was noticed at 5–22 min for all samples which then flattens as the time increases to 22–35 min. This might be due to the adsorbent reaching its maximum adsorption capacity. It can also be observed that adsorption of CO_2 was in the order BMAC > AMAC >UMAC, which infers that BMAC has the best adsorption capacity among the three samples investigated. This high adsorption capacity observed from BMAC could be attributed to its high surface area.

First-order kinetic model

The adsorption kinetics of the system was studied using the Lagergren pseudo-first-order model. Equation (5) was used to evaluate the adsorption dynamics
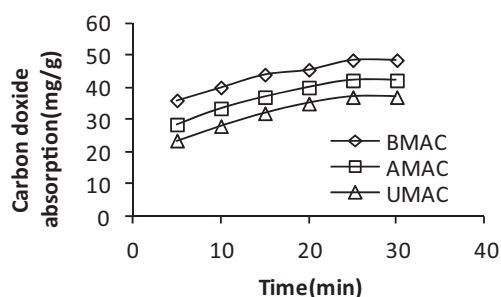

Figure 3. CO_2 adsorbed vs. time at a bed height of 6.5 cm (2 g), particle size of 8 mm^{-1}, temperature of 37°C and CO_2 flow rate of 60 ml/min.
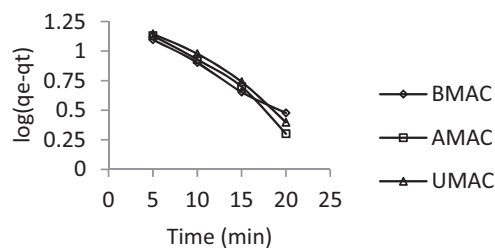

Figure 4. Pseudo-first-order kinetic model for CO_2 adsorption.

and its performance is shown in Figure 4 [9]. From Figure 4, it can be observed that, as the time increased, the values of log (qe-qt) decreased steeply at 5–17 min for all samples, while AMAC and UMAC tend to skew downwards. BMAC appears to have flattened downwards. R^2 values were BMAC = 0.9959, AMAC = 0.972, UMAC = 0.9758. The first order adsorption rate constants K were deduced to be KBMAC = 0.097, KAMAC = 0.1252, and KUMAC = 0.1140.

Pseudo-second-order model

Figure 5 shows a progressive increase of 1/qt (g.min^{-1}mg^{-1}) with t (min) for AMAC and UMAC in a straight-line form at 5–27 min. The adsorbent obeyed the second-order adsorption law with the following R^2: BMAC = 0.9965, AMAC = 0.9967, UMAC = 0.9928. The second-order adsorption rate constants K were as follows: K2BMAC = 0.0105, K2AMAC = 0.0052, K2UMAC = 0.0042

Pseudo-second-order model

Figure 6 shows the intra-particle diffusion model. Figure 6 clearly shows variation of gradient with respect to time. Two regions can be identified from Figure 6, the first steeper region at 2–4 $min^{1/2}$ and the second region at 4–5 $min^{1/2}$. According to Rashidi et al. [8], the first steeper region at that time range could be due to surface sorption, whilst the second region may be attributed to intra-particle diffusion. Since the gradients did not pass through the origin, it can be said that intra-particle diffusion is not the rate-limiting step in this adsorption. This observation can be compared with the reported literatures [8,32].
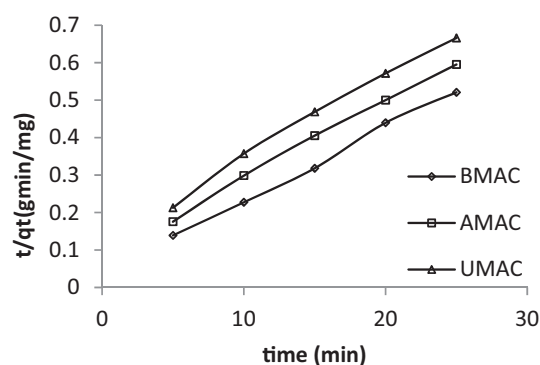

Figure 5. Pseudo-second-order kinetic model for CO_2 adsorption.

Table 4. Peak area of compounds identified from XRD analysis of BMAC before and after adsorption.

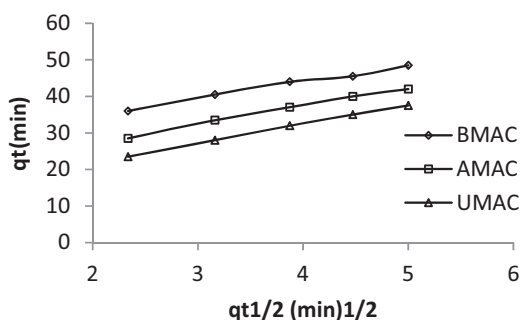| S/no	$2\theta(^0)$	compounds identified	% peak area before adsorption	% peak area after ad sorption
1	4	$NaSiO_3$	1.4	1.0
2	6	K_2CO_3	36.2	18.2
3	11	$Ca(OH)_2$	4	5.0
4	25	$C_2CaO_4.H_2O$	38.1	50
5	28	$Ca(PO_3)_2$	9.5	12.9
6	31	$3CaOSiO_2$	9.2	7.8
7	33	$CaCO_3$	1.6	5.1

Figure 6. Intraparticle diffusion model.

Kinetic parameters for carbon dioxide adsorption

In adsorption, the magnitude of the activation energy (E_a) according to Rashidi et al. [8] is an important parameter as it gives insight information on the mechanism of the adsorption process. Physical adsorption of CO_2 is associated with the formation of weak bonds between CO_2 and the activated carbon. This also requires less energy of formation resulting in low E_a which is usually within the range 5–40 kJ.mol^{-1}. In the chemisorption process, strong bonds are formed which require an energy of 40–800 kJ.mol^{-1} [22]. Table 4 shows that E_a for BMAC, AMAC and UMAC were 5.77, 13.02 and 13.55 kJ.mol^{-1}, respectively, which shows that this reaction was controlled by physio-sorption. The low E_a found in this work fell within the range stated in Özcan et al. [22]. This low E_a value implies that CO_2 adsorption onto activated carbon is diffusion controlled [8]. The results obtained in this study were significantly lower than 17.51 and 14.27 kJ.mol^{-1} reported for optimized and commercially available activated carbons, respectively, by Rashid et al. [8].

Fourier transform infrared analysis

FTIR analysis was used to study the changes in the functional groups of BMAC before and after adsorption as shown in Figure 7. The adsorption capacity of activated carbon is said to depend on the porosity and reactivity on the surface [33]. Figure 7 shows the absorbance is in the region 4000–400 cm^{-1}. Intermolecular
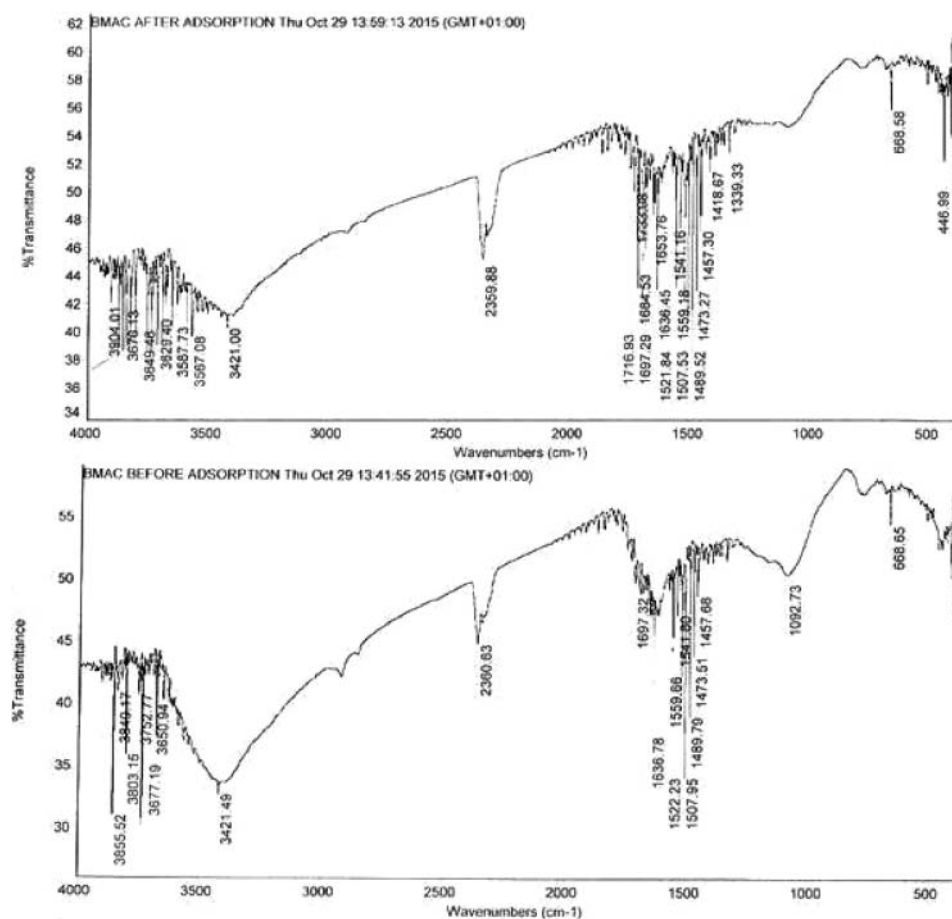
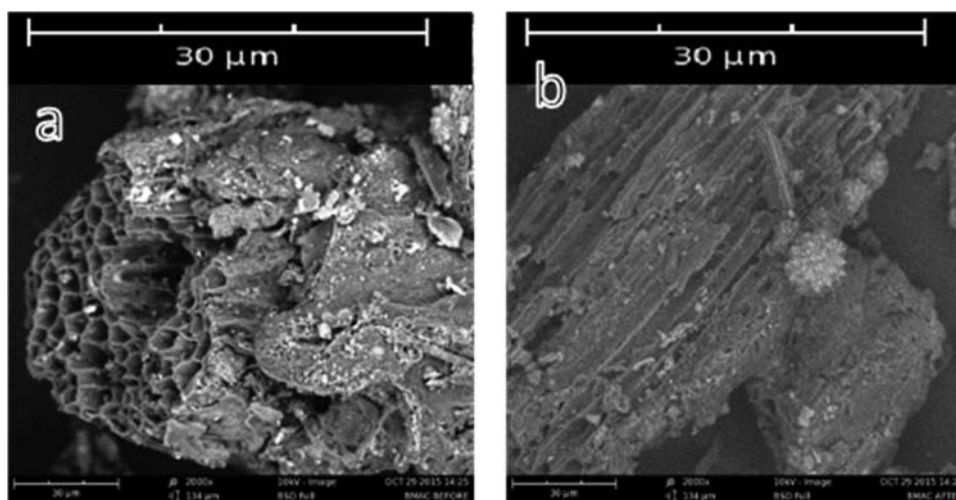

Figure 7. FTIR spectrum of BMAC before and after adsorption.

Figure 8. SEM micrographs of BMAC (a) before adsorption and (b) after adsorption.

bonded hydroxyl groups (OH) were observed at 3500–3200 cm^{-1} which increased after adsorption. Although the following peaks were observed to be common in both samples, the magnitude of the peaks is higher in the samples of the adsorbents after adsorption which is an indication that CO_2 had been adsorbed onto it.

The peaks observed from both adsorbents showed the following similarities: peak at 2905 cm^{-1} can be due to stretching vibration of C-H group; peaks around 1720 cm^{-1} could be due to the C = O group; and peak around 1620 cm^{-1} corresponded to C = C or asymmetric and symmetric stretching C = O vibrations. A strong C-O band observed at 1051 cm^{-1} was due to –OCH$_3$ group, showing the presence of lignin structure in the samples. The peak at 610 cm^{-1} was due to the bending modes of aromatic compounds, while peaks between 3640 cm^{-1} and 3610 cm^{-1} show the presence of alcohol and phenol functional groups [34]. Similar results were reported [33] for activated carbon produced from selected agricultural wastes.

Peaks at 1457.65, 1475.68, 1507.95 and 1527.2 cm^{-1} indicate the presence of alkynes, alkanes, and aromatic hydrocarbons. Peaks at 1541.8 and 1559.66 cm^{-1} indicate the presence of primary amines. These functional groups reflect the properties of the raw materials from which the activated carbon was synthesized. BMAC after adsorption showed peaks at 1339.33, 1418.67, 1457.27, 1507.53 and 1653.76 cm^{-1} which indicates the presence of alkyl halides, alkanes, nitrogenous compounds, and secondary and tertiary amines. The presence of amines and nitrogenous functional groups in BMAC after adsorption are an indication that CO_2 adsorption had taken place in the sample since nitrogenous and amine groups enhance CO_2 adsorption [25].

Scanning electron microscopy

A scanning electron microscope (SEM) was used to study the morphology of BMAC before and after

adsorption. It was observed that BMAC before adsorption showed visible pore sizes which are evident in Figure 8. The pores for BMAC after adsorption appeared less clear, which could be due to the adsorption of CO_2 gases into the visible pore spaces thus blocking the pores.

X-ray diffraction

Figure 9 shows X-ray diffraction (XRD) of BMAC before and after adsorption. The crystalline phases identified are quantified as shown in Table 5. Figure 4 shows that the activated carbon produced exhibits characteristic transformation from amorphous to orderly crystalline form. This conclusion was based on the absence of a well-known hunch back characteristic peculiar to amorphous material in the region between $2\theta = 10°$ and $22°$ [18,35]. It can be observed from Table 5 that the percentage area of the compounds identified had increased after adsorption confirming the adsorption of CO_2 onto the adsorbent. For example, at $2\theta = 33°$ the compound identified was $CaCO_3$ whose %peak area in the adsorbent was 1.6% and had increased to
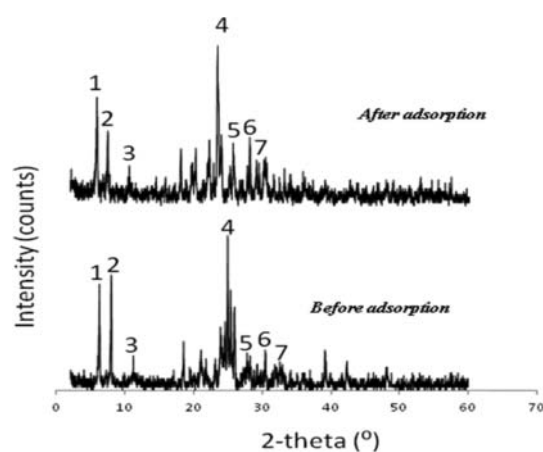

Figure 9. X-ray diffraction analysis of BMAC before and after adsorption.

Table 5. Peak area of compounds identified from XRD analysis of BMAC before and after adsorption.

S/no	$2\theta(^0)$	Compounds identified	% peak area before adsorption	% peak area after adsorption
1	4	$NaSiO_3$	1.4	1.0
2	6	K_2CO_3	36.2	18.2
3	11	$Ca(OH)_2$	4	5.0
4	25	$C_2CaO_4.H_2O$	38.1	50
5	28	$Ca(PO_3)_2$	9.5	12.9
6	31	$3CaOSiO_2$	9.2	7.8
7	33	$CaCO_3$	1.6	5.1

5.0% after adsorption. Also, $Ca(PO_3)_2$ was identified at $2\theta = 28°$ with %peak area of 9.5% which increased to 12.9% after adsorption. This increment could reflect the importance of base modification which opens more active sites for adsorption which is evident in the phosphate attachment to calcium, $Ca(PO_3)_2$. At $2\theta = 25°$, the compound identified was $C_2CaO_4.H_2O$, and its %peak area increased from 38.1% to 50%. The percentage increment of the peaks identified for the adsorbent after adsorption was 3.1%. This value 3.1% correlates well with the amount of CO_2 adsorbed at an optimum time of 35 min which was 4.8% when the difference can be compensated by the %peak area increment in the unidentified compounds.

Conclusions

CO_2 adsorption by UMAC, AMAC and BMAC from sugarcane bagasse was studied gravimetrically. Morphological structures and surface functional group of the adsorbent before and after the adsorption were studied and the results showed that BMAC had a better pore structure with unique surface properties which enable it to be most effective in CO_2 adsorption compared to AMAC and UMAC.

BMAC, AMAC and UMAC were produced from sugarcane bagasse and were found to be good adsorbents for CO_2 capture and sequestration. The adsorption capacity of the adsorbents was found to be in the order BMAC > AMAC > UMAC, with CO_2 adsorption capacities of 48.5, 42.2 and 37 mg.g^{-1} of adsorbent at 25 min and 25°C, which could be attributed to high surface area (800.6 $m^2.g^{-1}$) observed from BMAC as compared to 602.2 and 563.8 $m^2.g^{-1}$ for AMAC and UMAC. These values are higher than the literature reported values obtained from sugarcane bagasse subjected to the same experimental conditions but not modified with acid and base. These adsorbents also exhibited a good adsorption capacity for their various loading rates. From the equilibrium and kinetics of CO_2 adsorption studied, the magnitude of activation energies of the process were found to be less than 40 kJ.mol^{-1} (5.77, 13.02 and 13.55 kJ.mol^{-1} for BMAC, AMAC and UMAC) which indicates a physical adsorption mechanism. The second-order model R^2 value which is close to unity as compared to that of the first-order model showed that the adsorption of CO_2 onto the activated carbon obeys the pseudo-second-order model. A highly-porous activated carbon with high CO_2 adsorption capacity and lower activation energy produced from acid and base modified activated carbon from sugarcane bagasse in this research can be regarded as a better alternative adsorbent to both commercial and other activated carbons modified by methods such as amine impregnation.

Disclosure statement

No potential conflict of interest was reported by the author(s).

References

[1] Hileman B. Pace of global change quickens: Un report projects rapidly accelerating, Potentially devastating warning C&EN. 2001;79(5):1–9. available at: Cent/top-story/7905/7905notw1.html.

[2] Olivier J GJ, Janssens-Maenhout G, Muntean M, et al. Trends in global CO_2 emissions: 2015 Report, The Hague: PBL Netherlands Environmental Assessment Agency, Ispra: Europian Commission, Joint research center, PBL publication number: 1803 JRC Technical Note number: JRC98184 Trends in global CO_2 emissions: 2015 Report, 2015, 1–77.

[3] Herzog H, Eliasson B, Kaarstad, Eliasson O, Capturing greenhouse gases. Sci Am. 2000;282(2):72–79.

[4] Qiao H, Chen M, Meng L et al. Study on carbon dioxide removal from flue gas by absorption of aqueous ammonia, Third Annual Conference on Carbon Capture & Sequestration, Alexandria, VA, USA. Available from: https://www.netl.doe.gov/publications/proceedings/04/carbon-seq/158.pdf. 2004.

[5] D'Alessandro DM, Smit B, Long. RJ. Carbon dioxide capture: prospects for new materials. Angew Chem Int Ed. 2010;49:6058–6082.

[6] Murshid G, Shariff AM, Keong LK, et al. Thermo physical analysis of 2-amino-2-methyl-1-propanol solvent for carbon dioxide removal. Chem Eng Trans. 2011;25:45–50. DOI:10.3303/CET1125008.

[7] Plaza MG, Pevida C, Arias B, et al. A comparison of two methods for producing CO_2 capture adsorbents. Energy Procedia. 2009;1:1107–1113.

[8] Rashidi NA, Yusup S, Lam HL. Kinetic studies on carbon dioxide capture using activated carbon. Chem Eng Trans. 2013;35:361–366.

[9] Alhassan M, Auta M, Sabo JK, et al. CO_2 capture using amine –impregnated activated carbon from Jatropha Curcas Shell. Brit J. Adv Sci Technol. 2016;4(4):1–11

[10] Ketcha JM, Dina DJD, Ngomo HM, et al. Preparation and characterization of activated carbons obtained from Maize Cobs by Zinc Chloride Activation. Am Chem Sci J. 2010;2(4):136–160. Available from:www.sciencedomain.org

[11] Tsai WT, Chang CY, Lee SL. A low cost adsorbent from agricultural waste corncob by Zinc chloride activation. Biores Technol. 1998;64:211–217.

[12] Tsai WT, Chang CY, Chang CF, et al. Cleaner production of carbon adsorbents by utilizing agricultural waste corn cob. Resour Conserv Recy. 2001;32:43–53.

[13] Chang CF, Chang CY, Tsai WT. Effects of burn-off and activation temperature on preparation of activated carbon from corn cob agrowaste by CO2 and steam. J. Colloid Interf Sci. 2000;232:45–49.

[14] Boudrahem F, Aissani-Benissad F, Ait-Amar H. Batch sorption dynamics and equilibrium for the removal of lead ions from aqueous phase using activated carbon developed from coffee residue activated with zinc chloride. J. Environ Manage. 2009;90:3031–3039.

[15] Bansal RC, Donnet JB, Stoeckli HF. Active carbons. New York: Mercel Dekker; 1988. p. 482.

[16] Nabaisa V, Laginhas C, Carrott R, et al. Surface and porous characterisation of activated carbons made from a novel biomass precursor, the esparto grass. Appl Surf Sci. 2013;265:919–924.

[17] Williams TP, Reed RA. High grade activated carbon matting derived from the chemical activation and pyrolysis of natural fibre textile waste. J Anal Appl Pyrol. 2004;71 (2):971–986.

[18] Alhassan M, Andresen J. Effect of bone during fixed bed pyrolysis of pistachio nut shell. In J Al Sci Eng Invest. 2013;2(12):2251–8843.

[19] Pendyal B, Johns MM, Marshall WE, et al. The effect of binders and agricultural by-products on physical and chemical properties of granular activated carbons. Bioresource Technol. 1999;68:247–254.

[20] Al-Qodah Z, Shawabkah R. Production and characterization of granular activated carbon from activated sludge. Braz J Chem Eng. 2009;261:127–136.

[21] Alzaydian AS. Adsorption of methylene blue from aqueous solution onto a low – cost natural Jordanian Tripoli. Am J Appl Sci. 2009;6(6):1047–1058.

[22] Özcan A, Öncü EM, Özcan AS. Kinetics, isotherm and thermodynamic studies of adsorption of acid blue 193 from aqueous solutions onto natural sepiolite, colloids and surfaces. Physicochem Eng Aspect. 2006;277:90–97.

[23] Ho YS, Ng JC, McKay G. Kinetics of pollutant sorption by sorbents: Review, Separ Purif Rev. 2000;29:180–232.

[24] Sultana MS, Rahman MA. Characterization of calcined sugar cane bagasse ash and sugar cane waste ash for industrial use. International conference on Mechanical and Material Engineering (ICMIME2013); Nov 1–3; Bangladesh: RUET Rajashahi; 2013. p. 508–513.

[25] Takashi A, Takashi O, Kuniaki K, et al. Ammonia adsorption on bamboo charcoal with acid treatment. J Health Sci. 2006;52:585–589.

[26] Devnarain PB, Arnold DR, Davis SB. Production of activated carbon from South African sugar cane bagasse. Proc S Afr Sug Technol Ass. 2002;76:477–489.

[27] Smit B. EFRC-NETL research on carbon capture and ARPA-e, Us department of energy. Office of Basic Energy Sciences Energy Frontier Research Center 2015;1–5. available at: https://www.net.doe.gove/file%20library/events/2012/co2%capture%meeting/B-Smit-Berkley-Capture-Research.pdf.

[28] Yang T, Lua AC. Characteristics of activated carbons prepared from pistachio-nut shells by physical activation. J Coll Interf Sci. 2003;267:408–417.

[29] Rashidi NA, Yusup S, Borhan A. Development of novel low-cost activated carbon for carbon dioxide capture. Int J Chem Eng Appl. 2014;4(2):91.

[30] Qureshi K, Bhatti I, Kazi R, et al. Physical and chemical analysis of activated carbon prepared from sugarcane bagasse and use for sugar decolorization. Inte J Nat Sci Eng. 2008;1(3):145–149.

[31] Wu J. Modeling adsorption of organic compounds on activated carbon: a multivariate approach. Thesis, Umea, Sweden: Publised by Solfjadern offset AB. 2004. ISBN: 91-7305-697-9.

[32] Olu-Owolabi BI, Diagboya PN, Ebaddan WC. Mechanism of Pb^{2+} removal from aqueous solution using a non-living moss biomass. Chem Eng J. 2012;195-196:270–275.

[33] Khalil HPS, Jawaid M, Firoozian P, et al. Activated carbon from various agricultural wastes by chemical activation with KOH: preparation and characterization. J Biobase Mater Bioenerg. 2013;7:1–7.

[34] Coates J. Interpretation of infrared Spectra, a practical approach. In Meyers RA, editor. Encyclopedia of analytical chemistry. Chichester: John Wiley & Sons Ltd; 2000. p. 1–45.

[35] Govindarajan D, Jayalakshini G. XRD, FTIR and SEM studies on calcined sugarcane bagasse ash blended cement. Achieve Phys Res. 2011;2(4):38–44.